HHS Public Access

Author manuscript

Cell Rep. Author manuscript; available in PMC 2018 November 05.

Published in final edited form as:

Cell Rep. 2018 February 13; 22(7): 1695–1709. doi:10.1016/j.celrep.2018.01.007.

Activity Regulates Cell Death within Cortical Interneurons through a Calcineurin-Dependent Mechanism

Rashi Priya[1], **Mercedes Francisca Paredes**[3], **Theofanis Karayannis**[1,7], **Nusrath Yusuf**[1,5], **Xingchen Liu**[1], **Xavier Jaglin**[1,5], **Isabella Graef**[2], **Arturo Alvarez-Buylla**[3], and **Gord Fishell**[1,4,5,6,8,*]

[1]NYU Neuroscience Institute and Department of Neuroscience and Physiology, Smilow Research Center, New York University School of Medicine, 522 First Avenue, New York, NY 10016, USA

[2]Department of Pathology, Stanford University School of Medicine, Stanford, CA 94305, USA

[3]Department of Neurological Surgery, The Eli and Edythe Broad Center of Regeneration Medicine, Stem Cell Research, University of California, San Francisco, San Francisco, CA 94143, USA

[4]Center for Genomics and Systems Biology, New York University Abu Dhabi, Abu Dhabi, UAE

[5]Department of Neurobiology, Harvard Medical School, 220 Longwood Avenue, Boston, MA 02115, USA

[6]Stanley Center at the Broad Institute, 75 Ames Street, Cambridge, MA 02142, USA

Summary

We demonstrate that cortical interneurons derived from ventral eminences, including the caudal ganglionic eminence, undergo programmed cell death. Moreover, with the exception of VIP interneurons, this occurs in a manner that is activity-dependent. In addition, we demonstrate that, within interneurons, Calcineurin, a calcium-dependent protein phosphatase, plays a critical role in sequentially linking activity to maturation (E15–P5) and survival (P5–P20). Specifically, embryonic inactivation of Calcineurin results in a failure of interneurons to morphologically mature and prevents them from undergoing apoptosis. By contrast, early postnatal inactivation of Calcineurin increases apoptosis. We conclude that Calcineurin serves a dual role of promoting first the differentiation of interneurons and, subsequently, their survival.

In Brief

*Correspondence: gordon_fishell@hms.harvard.edu.
[7]Present address: Brain Research Institute, University of Zurich, Zurich, Switzerland
[8]Lead Contact

Author Contributions: R.P. and G.F. conceived the project. I.G. provided the *CnB fl/fl* mouse. R.P., M.F.P., T.K., X.L., N.Y., and X.J. performed the experiments. X.J. provided the AAVs. R.P. and G.F. wrote the manuscript with the help of all authors.

Declaration Of Interests: A.A.-B. is a co-founder and on the Scientific Advisory Board of Neurona Therapeutics.

Supplemental Information: Supplemental Information includes Supplemental Experimental Procedures and seven figures and can be found with this article online at https://doi.org/10.1016/j.celrep.2018.01.007.

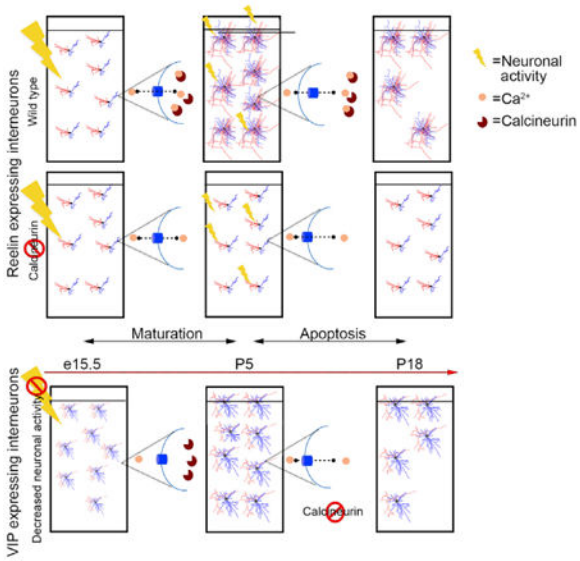

Priya et al. demonstrate that maturation and cell death within most populations of cortical interneurons is mediated by activity, which is transduced into intracellular signals through activation of the protein phosphatase Calcineurin. Thus, a single mechanism sequentially promotes interneuron differentiation and cell death in all interneurons except VIP-expressing cells.

Introduction

Inhibitory interneurons play a pivotal role in gating, sculpting, and preventing runaway excitation within the cortex. Although inhibitory interneuronal populations are less numerous than their excitatory counterparts, they are comprised by an extremely broad variety of subtypes (Butt et al., 2005; Lee et al., 2010; Miyoshi et al., 2010; Xu et al., 2004). This heterogeneity reflects their functional diversity, which allows them to collectively fine-tune the flow of cortical information while maintaining excitatory/inhibitory balance (Haider et al., 2006; 2013; Pouille and Scanziani, 2001; Wehr and Zador, 2003).

The stereotypic organization of cortical circuits demands that a broad range of interneuron classes integrate in appropriate numbers. This requires a tradeoff between the need to maintain subtype heterogeneity without imposing too great a cost on resources. We recently hypothesized that the refinement of interneuron subtypes within the cortex occurs after they have reached their settling positions, whereupon instructive local cues allow them to achieve their definitive functional identity (Kepecs and Fishell, 2014). For such a regulative strategy to be precise, the cortex must rely on a buffering capacity in the form of neuronal overproduction. In support of this general hypothesis, recent work has shown that ~30% of the initial population of medial ganglionic eminence (MGE)-derived cortical interneurons undergo cell death (Southwell et al., 2012). However, the extent to which cell death also affects the cortical interneuron population derived from the caudal ganglionic eminence (CGE) (Lee et al., 2010) and the exact mechanism by which the apoptotic pathway is controlled in developing interneurons remain to be elucidated.

In nematodes, pioneering work from the Horvitz laboratory revealed that a precise cell intrinsic genetic cascade mediates programmed cell death (Cameron et al., 2002; Conradt and Horvitz, 1998; Horvitz, 2003; Sulston and White, 1980). Cell death in higher vertebrates is initiated through a variety of mechanisms, including competition for trophic support (Levi-Montalcini, 1987; Oppenheim, 1989; Oppenheim et al., 1993) as well as cell-autonomous mechanisms (Southwell et al., 2012). Within interneuronal populations, the number of neurons that survive cell death scales with the initial size of the progenitor population (Southwell et al., 2012).

Here we demonstrate that neuronal activity modulates interneuron survival, with decreased activity increasing cell death and increased activity diminishing it. Our work confirms recent work showing a more general requirement for activity for cell survival in the primary sensory cortex (Blanquie et al., 2017). It is also consistent with a paper in this issue of *Cell Reports* showing a requirement for activity for interneuron survival (Dexana et al., 2018). This latter study, like ours, discovered that, in vasointestinal peptide (VIP), interneurons, although they undergo apoptosis, survival is not regulated by activity. A growing body of literature indicates that calcium influx couples excitation to a variety of biological processes (Bando et al., 2016; Bean, 1989; Bonci et al., 1998; Brosenitsch and Katz, 2001; Mermelstein et al., 2000; Tsien et al., 1988; Wheeler et al., 2012; Yasuda et al., 2003), including transcription and alternative splicing (Ghosh and Greenberg, 1995; Greenberg et al., 1986; Iijima et al., 2011). We discovered that, with the exception of VIP cells, activity in interneurons directly modulates the activity of the phosphatase Calcineurin (CaN) and is sequentially required for maturation and survival.

Results

Cell Death in CGE-Derived Interneurons Is Bax-Mediated

Cortical interneurons derived from the MGE have been shown to undergo 20%–40% apoptosis between the first and second postnatal weeks (Southwell et al., 2012). However, the extent to which cell death occurs in CGE-derived interneuron populations has not been previously examined. We assessed this by monitoring changes between birth and the second postnatal week using a *5HT3aR*^{eGFP} transgenic line, which labels all CGE-derived interneurons (Lee et al., 2010). At both post-natal day 5 (P5) and P21 we comprehensively quantified the number of CGE interneurons within the anterior-posterior axis of the cortex. Our analysis revealed that the number of CGE-derived interneurons decreased by approximately 20% between these time points (Figures 1A and 1B).

Because CGE-derived interneurons as a population are generated later than MGE-derived interneurons (Miyoshi et al., 2007, 2010), we wanted to determine whether the peak in their cell death is shifted accordingly. To address this question, we analyzed the number of CGE-derived interneurons that are positive for cleaved caspase-3 at different time points, revealing that the peak of cell death was P9 (Figure 1C).

Next, we crossed the *5HT3aR*^{cre} mouse line with a *Bax*^{fl} allele and examined the proportion of cell death in the two primary subtypes within the CGE population, those expressing VIP or Reelin (Butt et al., 2005; Lee et al., 2010; Miyoshi et al., 2010). We found a significant

increase in the numbers of both VIP-and Reelin-expressing interneurons in the cortex of *Bax*-null animals compared with their control littermates (Figures 1D–1F).

Neuronal Activity Differentially Modulates Cell Death within CGE-Derived Interneuron Populations

Given that the morphological maturation and functional integration of interneurons is coincident with the onset of activity (Allène et al., 2008; Close et al., 2012; De Marco García et al., 2011; 2015) and recent evidence that activity regulates cell survival in the somatosensory cortex (Blanquie et al., 2017), we decided to investigate whether activity per se regulates apoptosis. To test this possibility, we sought to dampen levels of activity within interneurons *in vivo*. To reduce neuronal activity in cortical interneurons, we unilaterally injected into the somatosensory cortex of 5HT3aR^{cre} animals an adeno-associated virus (AAV) driving the expression of Kir2.1-P2A-mCherry. Kir2.1 is an inward-rectifying potassium channel that hyperpolarizes neurons (De Marco García et al., 2011; Yu et al., 2004), which we fused to mCherry by P2A, and regulated by a cre-dependent genetic switch (flip-excision [FLEx] switch) (hereafter referred to as AAV-EF1:DIO:Kir2.1-P2A-mCherry). These experiments were done on a background containing the R26R CAG-boosted EGFP (RCE):LoxP reporter. As a control, we unilaterally infected the cortex with AAV-EF1:DIO:mCherry in 5HT3aR^{cre}; RCE:LoxP littermates. Under both conditions, animals were injected at P0/P1 and sacrificed at P18 (Figure 2A). The expression of Kir2.1-mCherry initiates around P5 (data not shown), a time point corresponding to the onset of the period of physiological cell death in the developing cortex. The number of GFP+ interneurons in the injected hemisphere were counted and compared with the AAV-flex-mCherry-injected control condition. We observed that the numbers of GFP+ neurons in the Kir2.1-expressing hemisphere were significantly reduced by 9% (Figures 2B and 2C). We examined the two most prominent CGE interneuron types expressing Reelin and VIP. Interestingly, although the numbers of Reelin-expressing interneurons were diminished within Kir2.1- expressing populations, the number of VIP-expressing interneurons compared with the control was unchanged (Figures 2D–2G).

Next, we wanted to determine whether activity also regulates cell survival within the entire interneuron population. To address this question, we unilaterally injected our AAV-EF1:DIO: Kir2.1-P2A-mCherry virus into the somatosensory cortex of compound *Dlx6a^{cre};RCE:LoxP* animals, in which the entire population of cortical interneurons is EGFP + (Yu et al., 2011). As a control, we again infected the cortex of *Dlx6a^{cre};RCE:LoxP* animals with AAV-EF1:DIO:mCherry. We found a 20% decrease in EGFP+ interneurons in the region in which Kir2.1 expression was expressed (Figures S2A and S2B).

In a complementary set of experiments, we increased the level of activity in these same populations of interneurons by using bacterial sodium channel (NaChbac), a bacterial voltage-gated sodium channel that decreases the threshold for firing (Bando et al., 2016; Lin et al., 2010). This channel was incorporated into an AAV-flex-P2A-mCherry vector (AAV-EF1:DIO:NaChbac-P2A-mCherry). We found that the unilateral injection of the AAV-EF1:DIO:NaChbac-P2A-mCherry virus into the cortex of *Dlx6a^{cre};RCE* animals led to a 20% increase in the survival of GFP+ cortical interneurons (Figures S2A and S2B)

compared with the control. We also found an increase in the number of Reelin-expressing interneurons in cortices injected with AAV-flex-NaChbac-P2A-mCherry. However, the number of VIP-expressing interneurons remained unaltered (Figures S2C and S2D).

To more rigorously ascertain whether the lack of influence of activity on survival was specific for VIP-expressing interneurons, we tested the effects of dampened neuronal activity on the two major subtypes of MGE-derived interneurons. We assessed the number of parvalbumin (PV)-expressing and somatostatin (SST)-expressing neurons when the entire interneuron population was targeted with Kir2.1. As with Reelin cells, we also observed a reduction in the numbers of both PV- and SST-expressing cells in hemispheres expressing the AAV-Kir2.1-mCherry construct (Figures S2E and S2F) compared with the control. This suggests that VIP-expressing interneurons are the sole class of cortical interneurons in which cell death is not regulated by activity.

Interneuron Survival Does Not Depend on Soluble Signals from Glia or Neurons

Despite identifying a role for neuronal activity for the regulation of cell death, we sought to investigate whether other factors also contribute to survival during apoptosis. Brain derived neurotrophic factor (BDNF) is one of the best-studied neurotrophic factors released from neurons and is involved in various developmental processes, including cell survival (Ghosh et al., 1994; Kokaia et al., 1993; Miller and Kaplan, 2001; Polleux et al., 2002; Riccio et al., 1999). Previous investigators had already reported that the removal of the BDNF receptor TrkB did not have any effect on the cell survival of MGE-derived interneurons (Southwell et al., 2012). However, BDNF can also activate the p75 receptor (McKay et al., 1996). We therefore wanted to test whether BDNF itself affects interneuronal survival. We found that treatment of *GAD67*^{GFP}-labeled interneurons with BDNF *in vitro*, although it had an effect on the neurite outgrowth, did not increase the survival of interneurons compared with untreated controls (Figures S3A and S3B). We next wished to assess whether other still un-identifiedglia- orneuron-derived factors may mediate interneuron survival. Indeed, the presence of a cortical feeder layer is critical for the survival of cortical interneurons *in vitro*, suggesting that some aspect of cell-cell interactions must regulate survival during the cell death period (Xu et al., 2004). Glia have been previously reported to provide a permissive substrate for neuronal development (Henderson et al., 1994; Jin et al., 2002; Lin et al., 1993). To address whether this is true for interneurons, we placed embryonic day 13.5 (E13.5) *GAD67*^{GFP}-labeled cells onto a P0–P2 glial feeder layer (Figure S3C) and measured their survival. We found that the number of GFP^{+} neurons *in vitro* declined steeply over time (Figure S3D). This suggests that glia alone are not sufficient to support cortical interneuron survival.

We next examined whether secreted factors from neuronally conditioned medium might prove to be more efficacious in promoting interneuronal survival *in vitro*. However, the presence of medium conditioned by neurons did not rescue the decline in the number of interneurons placed on the glial feeder layer (Figure S3E). Therefore, neither glia nor soluble factors secreted from neurons are sufficient to promote the survival of developing interneurons *in vitro*. To assess whether the influence of the cortical feeder layer was dependent on neuronal activity, we subjected cultured neurons plated on the neuronal feeder

layer to tetrodotoxin (TTX), which blocks voltage-gated sodium channels. This resulted in survival comparable with cultured neurons lacking a cortical feeder layer (Figures S3F and S3G). By contrast, when activity was augmented in these populations by subjecting interneurons to K^+ enriched solution (25 mM), we observed a trend toward increased survival (Figures S3F and S3G). These findings support our hypothesis that neuronal activity promotes the survival of interneurons.

Activity Levels that Reduce Cell Death Result in Activation of the Calcium Effector CaN

The pattern of NaChbac-induced firing, which reduced the degree of cell death in interneurons (Figures S4A and S4B) resemble early cortical network oscillations or giant depolarizing potentials (Allène et al., 2008; Khazipov et al., 2004) that occur when a cluster of action potentials result in intracellular calcium influx (Bando et al., 2016; Lin et al., 2010). Both with NaChbac and *in vivo*, these bursts occur at a frequency of about 1 mHz (Figure S4C), which has been shown previously to favor CaN activation (Dolmetsch et al., 1998). CaN is a phosphatase that regulates several synaptic and transcriptional pathways. Its high affinity for calcium (Klee et al., 1979) makes it a strong putative candidate as the effector molecule that is activated upon bouts of neuronal activity. However, previous findings suggest that CaN is not expressed in hippocampal interneurons (Sík et al., 1998). To establish the presence of CaN in cortical interneurons, we utilized the *5HT3aR-BAC*^{eGFP} and *Lhx6*^{eGFP} mouse lines to label CGE- and MGE-derived interneurons, respectively. EGFP+ neurons were sorted by fluorescence-activated cell sorting (FACS) and biochemically treated for the extraction of cellular proteins. The resulting lysates were subjected to western blotting to stain for the regulatory subunit of CaN (Cnb), the isoform that is enriched in the brain (Chang et al., 1994; Ueki et al., 1992). Our results indicate that both CGE- and MGE-derived interneurons express the regulatory subunit of CaN (Figure S4D).

CaN is a heterodimer that depends upon the β-regulatory subunit interacting with a catalytic subunit. The catalytic subunit has multiple isoforms, each encoded by separate genes. To identify the possible isoforms that could be utilized within interneurons, we used the *Dlx6a*^{cre}*; RCE* mouse line to isolated interneurons from the cortex using FACS. The cell lysates obtained were analyzed by western blot using antibodies against the catalytic subunit alpha isozyme (CNA1), beta isozyme (CNA2), and gamma isozyme (CNA3). Our results indicate the presence of all three CNA isoforms in interneurons (Figures S4E and S4F).

We next sought to determine whether CaN is activated by neuronal excitation in interneurons. We first asked whether enhanced neuronal activity in interneurons results in dephosphorylation of dynamin1, a well-recognized target of CaN. This CaN target is involved in activity-dependent bulk endocytosis and becomes dephosphorylated during bouts of elevated neuronal activity (Clayton et al., 2009; Evans and Cousin, 2007). To this end, we utilized *Dlx6a*^{cre}*;Ai9* (*ROSA 26Sor* locus [RCL]-tdTomato), P7 pups and subjected them to either electroconvulsive shock (ECS) to globally and acutely increase the level of neuronal activity within the brain (Daval et al., 1989; Guo et al., 2011) or sham treatment. The animals were then sacrificed 3 hr after induction. td-Tomato-positive interneurons from the cortex were sorted by FACS and biochemically treated to extract proteins, which were

subjected to western blotting and quantified for the level of S774 phospho-dynamin 1. We found that ECS-treated animals had dramatically reduced levels of phospho-dynamin 1 compared with sham-treated pups, suggesting that CaN is involved in the dephosphorylation of dynamin 1 in inter-neurons during bouts of increased neuronal activity (Figures 3A and 3B). ECS can also result in more general effects on both mitochondria and the endoplasmic reticulum. Therefore, one must remain cautious in interpreting changes as stemming solely from alterations in activity.

To specifically examine VIP+ interneurons that are refractory to activity, we examined dynamin dephosphorylation in VIP inter-neurons using a *VIP^{cre}* mouse line crossed with the Ai9 (RCL-td-Tomato) reporter line. Although VIP+ interneurons express CaN (Figure S4G), we observed no change in the levels of phospho-dynamin 1 upon ECS treatment compared with sham treatment (Figures S4H and S4I).

To validate dynamin 1 as a *bona fide* target of CaN in interneurons, we examined the level of phosphorylation of this protein upon *Cnb* loss of function. The *Cnb* gene was conditionally removed within interneurons by crossing a conditional *Cnb* allele onto a compound *Dlx6a^{cre};RCE* mouse background (subsequently referred to as *CnB cKOs)*. Interneurons from *cKOs* versus control mice were isolated, lysed, and probed for S774 phospho-dynamin 1. Consistent with dynamin 1 being a direct target of CaN, we found that the level of phospho-dynamin 1 was substantially increased in *Cnb cKOs* compared with wild-type mice (Figures S4J and S4K).

To confirm the relationship of activity level with CaN activation, we examined another downstream target of CaN, nuclear factor of activated T-cells, cytoplasmic (NFATc), a transcription factor (Clipstone and Crabtree, 1992; Flanagan et al., 1991). NFATc is translocated to the nucleus in neurons upon CaN activation (Beals et al., 1997; Flanagan et al., 1991; Graef et al., 1999). To determine whether such a translocation occurs, we injected *Dlx6a^{cre}* animals at birth with the AAV-flex NaChbac-P2A-mCherry, which were then sacrificed at P7 and immuno-stained for NFATc4. We observed that AAV-flex NaChbac-P2A-mCherry expression in interneurons results in the nuclear localization of NFATc4 (Figures 3C and 3D). By contrast, the levels of nuclear NFATc4 decreased upon the expression of AAV-flex Kir2.1-P2A-mCherry in interneurons (Figures 3C and 3E). Taken together these findings are consistent with our hypothesis that CaN signaling is recruited upon neuronal activation and may be involved in regulating the cell death response.

Embryonic Inactivation of CaN Results in an Increase in the Number of Cortical Interneurons

We next used both pharmacological and genetic strategies to directly assess whether CaN regulates cell death in cortical interneurons. We began by suppressing the enzymatic activity of CaN at the peak of cell death using FK506, a pharmacological blocker (Sussman et al., 1998). We unilaterally injected FK506 diluted in DMSO or vehicle control into the P7 somatosensory cortex, along with red fluorescent beads to identify the site of injection. These experiments were performed on *Dlx6a^{cre};RCE* mice. We compared the number of GFP+ neurons within the FK506-injected and vehicle-injected hemispheres and found that they were decreased 20% within the FK506-injected side compared with the control

hemisphere (Figures S5A–S5C). However, pharmacological blockade non-specifically removes CaN function in all cortical cells. To directly demonstrate that CaN is required cell-autonomously for interneuronal cell survival, we next used a genetic strategy where CaN was selectively removed from interneurons by crossing a *Cnb*$^{fl/fl}$ allele with the *Dlx6a*^{cre} driver. This conditional genetic knockout of *Cnb* resulted in increased mortality after P14 and fully penetrant lethality by P22 (Figure 4A). Additionally, the animals were smaller in size and had reduced body weight compared with their control littermates (Figure S5D). Interestingly, we found that, even though overall body size was significantly smaller compared with the controls, the size of the brain and cortical thickness were equivalent to that seen in control littermates (Figures S5E and S5F). At P18–P21, the number and distribution of GFP+ interneurons was equivalent within heterozygous and wild-type animals (Figure S5G); therefore, we used the *Dlx6a*^{cre}*; Cnb*$^{fl/+}$*; RCE* animals as controls. Surprisingly, by P18–P21 in *Dlx6a*^{cre}*;Cnb*$^{fl/fl}$*;RCE* animals, we found that the number of GFP+ neurons was increased by 20% compared with the control littermates (Figures 4B and 4C), and that increase was most marked specifically in superficial layers (Figure 4D). Additionally, we observed a decrease in the cumulative cleaved caspase-3 immunoreactivity in *Cnb* conditional knockout (cKO) animals at P7 (Figure S5H). To confirm that the increase in the number of GFP+ neurons was not due to migration/dispersion issues along the rostral-caudal axis, we compared sections from the motor, somatosensory, and visual areas and observed that the increase in the number of neurons was consistent throughout the cortex (Figures S5I and S5J). To determine whether the increase in the number of interneurons upon *Cnb* removal was due to an increase in proliferation, we analyzed the number of GFP+ neurons at P5. This represents a developmental stage by which all cortical interneurons have settled within the cortex but cell death phase has yet to commence. Hence, this is the time point at which the cortical interneuron population reaches its maximum. Arguing against changes in proliferation as a result of *Cnb* removal, we did not observe any significant difference in the numbers of interneurons at P5 between the cKO animals and the controls (Figures S5K and S5L). To validate the loss of the Cnb gene from *Dlx6a*^{cre}*;RCE* labeled interneurons, we performed an *in vitro* analysis by co-immunostaining for CnB and GFP (Figure S5M). These results suggest that the increase in number of neurons is due to a decrease in cell death in the developing cortex upon embryonic *Cnb* removal.

The Increased Survival of Interneurons upon Embryonic Removal of Cnb Is Not Due to an Increase in Electrical Activity

Our work indicates that CaN's phosphatase function in interneurons could be induced by electrical activity. We also have shown that increasing activity within interneurons promotes their survival. We were therefore surprised to find that embryonic loss of *CnB* in interneurons in fact increased interneuron survival (Figure 4C). One possibility is that the increase in the number of interneurons upon embryonic removal of *Cnb* is due to homeostasis, resulting in an increase in excitatory postsynaptic currents (Baumgärtel and Mansuy, 2012; Beattie et al., 2000; Kim and Ziff, 2014; Lieberman and Mody, 1994). Indeed, by performing electrophysiological recordings of spontaneous excitatory postsynaptic currents (sEPSCs) onto layer 1 interneurons, we found that there was a significant increase in the number and amplitude of sEPSCs in interneurons lacking *Cnb* gene function compared with control cells (Figures 5A–5C). We therefore investigated

whether autonomously dampening neuronal activity in interneurons in *Dlx6a^{cre};Cnb$^{fl/fl}$;RCE* animals could reverse the increased interneuronal survival. To address this question, we unilaterally injected the cortex at P0/P1 with AAV-flex Kir2.1-P2A-mCherry in embryonic *Cnb* knockout pups (Figure 5D). However, even when the increased excitation of *Cnb*-null interneurons was abrogated through Kir2.1 overexpression, we still observed increased survival in *Cnb* knockouts (Figures 5E and 5F) compared with the controls. These data suggest that the increased numbers of interneurons under embryonic *Cnb* knockout (KO) conditions is not due to the concomitant increase in their activity associated with loss of CaN function.

Early Removal of CaN Prevents the Maturation of Interneurons

Previous work indicated that interneurons do not undergo cell death before they reach a certain stage of maturation (Southwell et al., 2012). That led us to hypothesize that CaN might be involved in the maturation of interneurons and that its absence could suppress their progression to the developmental stage at which apoptosis is initiated. Using *in utero* electroporation, we sparsely targeted CGE-derived interneurons so that only cell-autonomous effects would be evident. *Dlx5/6:eGFP*- and *Dlx5/6:cre*-containing plasmids were co-electroporated into E15.5 *Cnb$^{fl/+}$* and *Cnb$^{fl/fl}$* embryos (a vector and time point that favor the targeting of CGE interneurons; De Marco García et al., 2011), and the labeled cells were analyzed at P8 (Figure 6A). We found that the morphology of *Cnb$^{fl/fl}$* Reelin-expressing interneurons was stunted as a result of *Cnb* removal (Figures 6B, 6D and 6F–6I). We also found the morphology of PV- and SST-expressing interneurons to be immature in *Cnb cKO* animals (data not shown). Consistently, the morphology of VIP-expressing interneurons was comparable with controls (Figures 6C, 6E and 6J–6M). Thus, the activation of CaN in CGE interneurons correlates precisely with a requirement for activity in cell survival. To explore other maturation properties of the interneurons that lack CaN, we undertook electrophysiological recordings of spontaneous inhibitory postsynaptic currents (sIPSCs) of layer 2–3 pyramidal cells within the barrel cortex of *Cnb* cKOs. We found that there was a significant reduction in the frequency and amplitude of sIPSCs in pyramidal neurons in *CnB* cKOs compared with that observed in wild-type animals (Figures S6A and S6B). This was not due to defects in the action potential generation within control versus cKO interneurons because analysis of the firing patterns revealed no major differences. Interestingly, we also found that the Reelin, a marker indicative of maturation in neurogliaform neurons, progressively diminishes in *Cnb* cKOs, reaching 50% of normal levels by P18 and only 5% byP21 (Figures S6C and S6D). By contrast, in these mutants, the VIP marker appeared to be unaffected (Figure S6E). Taken together, these data indicate a requirement for CaN in the maturation of Reelin-expressing interneurons prior to the onset of cell death.

Timing of CaN Removal Is a Critical Factor in Determining the Final Population Size

We showed that embryonic inactivation of CaN prevents cell death and alters maturation. However, pharmacological blockade of CaN during the postnatal period increased cell death. We finally wanted to test whether the differential response between the pharmacological blockade and *Cnb* cKO is due to the difference in the timing of *Cnb* removal (i.e., P7:FK506 versus E15:*Dlx6a^{Cre}*). We conditionally removed CaN function at the same age at which we

had previously administered FK506. Tamoxifen injection at P5/P6 of *Dlx1/2*^{creER};*Cnb*$^{fl/fl}$;*RCE* mice deleted the *Cnb* gene in interneurons. Indeed, we found that later removal of Cnb led to a decrease in the number of GFP+ interneurons, as seen with pharmacological treatment (Figures 7A–7C). Together, these results suggest a dual and sequential requirement for CaN in morphological development and the regulation of cell death in interneurons (Figures S7A and S7B).

Discussion

Our results show that activity-mediated calcium signaling involving CaN plays a pivotal role in the control of interneuronal cell death within all but the VIP^{+} subpopulation. Within interneurons where CaN-mediated activity regulates cell death, our findings indicate that it occurs in two stages: an early phase, during which CaN is required for morphological development, and a later period, when it acts to prevent cell death (for a model, see Figures S7A and S7B).

Previous work argues against interneuron survival being trophic factor-dependent (Southwell et al., 2012). In particular, the observation that a constant proportion of interneurons undergoes cell death when their numbers are considerably supernumerary (Southwell et al., 2012) is not consistent with such a mechanism. By demonstrating that activity regulates cell death, our present results provide a parsimonious explanation for the puzzling observation that the level of cell death among interneurons is proportional but scalable (Southwell et al., 2012). Neuronal activity is ideally suited to this task because there is no absolute limit to net activity. Indeed, studies done in the mouse olfactory and hippocampal systems, both of which are notable for their ability to incorporate new neurons throughout life, provide object examples of this principle (Doetsch et al., 1999; Gage, 2000; Lois et al., 1996; Song et al., 2002). In both of these instances, adult born neurons are able to continuously integrate into already established circuits in a manner that is both robust and essential for proper neural function (Alvarez-Buylla et al., 1990; Gage and Temple, 2013; Lin et al., 2010; Sahay and Hen, 2007).

Our results are also consistent with our working hypothesis that interneuron maturation is regulated by a two-step process: a genetically controlled specification step that we call cardinal specification and a secondary step that occurs post-migration, which we call definitive specification (Kepecs and Fishell, 2014). Specifically, we predict that determination of an interneuron's selection of afferent and efferent targets only occurs upon reaching their settling position. For such a mechanism to function, an error correction process is required to ensure that, if they are not properly integrated into cortical circuitry, then they are ablated (Figure S7B, model). Activity-mediated cell death provides an ideal mechanism to control such a process.

Numerous studies have emphasized the importance of activity in neuronal maturation (Polleux et al., 2007; West and Green-berg, 2011). With regard to interneurons specifically, previous work from our lab has shown a requirement for neuronal activity for their appropriate migration and morphological maturation (De Marco García et al., 2011). Our work now demonstrates that CaN provides a direct link between activity and cell death.

Moreover, the dual role for CaN in maturation and cell death shows how activity is sequentially coupled to both. This idea is supported by previous data where, with heterochronic transplantation of young interneurons, they only undergo apoptosis when they reach a particular chronological age and, hence, maturation (Southwell et al., 2012).

Our hypothesis is also consistent with a recent study that has shown that the conditional removal of *Dicer*, which is required for the production of miRNAs (Tuncdemir et al., 2015), concomitantly results in both their premature maturation and initiation of apoptosis. Thus, the apparent coupling of maturation and survival appears to represent a developmental checkpoint by which appropriate circuit integration is regulated.

Interestingly, with regard to the coupling of activity and cell death, VIP interneurons are the exception (De Marco García et al., 2011; 2015). Although they experience an equivalent degree of developmental cell death, this process is not activity-dependent. Interestingly, a number of features, most notably their function in disinhibition and their receipt of long-range inter-cortical projections (Fu et al., 2014; Lee et al., 2013; Pi et al., 2013), indicate that they play a unique role in cortical processing. Perhaps their involvement in recurrent cortical signaling rather than the processing of ascending sensory input results in VIP cell death being under trophic rather than activity-mediated control. Support for this idea comes from a recent study showing that VIP-expressing interneurons display an experience-induced gene expression program involving insulin-like growth factor (Mardinly et al., 2016).

In summary, our data demonstrate that the regulation of activity-mediated cell death is mediated through CaN signaling. We can now add survival to the list of findings showing that activity is essential for the migration (Polleux et al., 2002), morphological development (De Marco García et al., 2011), positioning (Lodato et al., 2011), and physiological properties (Dehorter et al., 2015).

Experimental Procedures

Mouse Strains

Strains from The Jackson Laboratory used in this study include Swiss Webster, *RCE:LoxP* reporter allele, $Bax^{fl/fl};Bak^{-/-},5HT3aR^{cre}$, $Bax^{fl/fl};Bak^{-/-};Lhx6^{cre}$ and $GAD67^{GFP}$ mice (a gift from the Yanagawa labs), Cnb^{fl} (I. Graef), $Dlx6a^{cre}$ (Yu et al., 2011), $Dlx1/2^{creER}$ (Batista-Brito et al., 2008), $5HT3aR\text{-}^{eGFP}$ (Gensat), $Lhx6\text{-}^{eGFP}$, and $5HT3A^{Cre}$ (a gift from N. Henitz, Rockefeller University) mouse lines. Temporal regulation of *Cnb* removal was obtained by cre^{ER} induction using tamoxifen administration (20 mg/mL in corn oil; 50-100 μL per pup) by intraperitoneal injections at selected time points (P6 and P7). Both males and females were used for all experiments. All animals were treated in accordance with the regulations and guidelines of the Institutional Animal Care and Use Committees at New York University School of Medicine and University of California, San Francisco.

Virus Injections

350 nL of Cre-regulated AAV containing mCherry-tagged Kir2.1 or NaChbac were injected unilaterally into the cortex at P0. The expression of mCherry was monitored to identify the kinetics of the viral expression. It took around 4–5 days for the expression of mCherry. For

the injections, animals were anesthetized by inducing hypothermia on ice. The pups were returned to the mother, sacrificed for further analysis at P18, and analyzed using cryostat sections for cell count or vibratome sections for electrophysiology.

In Utero Electroporation

The protocol for mouse *in utero* electroporation has been described elsewhere (De Marco García et al., 2011, 2015; De Marco Garcia and Fishell, 2014). The *Dlx5/6-cre* and *Dlx5/6-eGFP* plasmids were co-electroporated at E15.5 in embryos obtained from a $Cnb^{fl/+}$ and $Cnb^{fl/fl}$ cross. The controls were littermates. Mouse colony maintenance and handling were performed in compliance with the protocols approved by the Institutional Animal Care and Use Committee of the New York University School of Medicine.

FACS and Protein Analysis

Animals of the desired genotype, aged P7–P10, were sacrificed. Cortical sections were obtained and dissociated using a previously published protocol (Hempel et al., 2007). Dissociated cells from the cortical slices were then subjected to FACS (MoFlo, Beckman Coulter) to obtain EGFP+/td-Tomato interneurons. On average, the percentage of GFP+ interneurons was 2% –5% for P7–P10 ages. Collected cells were subsequently used to obtain protein by lysing in radioimmunoprecipitation assay (RIPA) buffer (50 nM Tris [pH 8.0], 150 mM NaCl, 1 % Triton X-100, 0.10% SDS, and 1 mM EDTA, water-adjusted to 100 mL). The protein was analyzed by western blot. The blots were blocked with 5% milk and probed for an antibody mix consisting of Rb-Cnb (Upstate Cell Signaling, 07-069, 1:1,000), m-α-actin (1:2,000), Rb-S774 Dynamin 1 (Abcam, ab55324, 1:1,000), total dyna-min 1 (Abcam, ab3456, 1:1,000), Rb-CNA1 (Millipore, 07-1490, 1:500), Rb- CNA2 (Abcam, ab96573, 1:500), and Rb-CNA3 (Abcam, ab154863, 1:1,000). Blots were imaged using an Odyssey CLx infrared imager and analyzed using ImageStudio software (LI-COR Biosciences) or using the enhanced chemiluminescence method. Fluorescent signaling for Cnb was normalized using β-actin.

Immunohistochemistry

Brains were fixed by transcardiac perfusion followed by 1 hr of postfixation on ice with 4% formaldehyde/PBS solution. Brains were rinsed with PBS and cryoprotected by using 30% sucrose/PBS solution overnight at 4°C. Cryosections were prepared at 20 μm (for counting immunoprofiles) thickness. Immunohistochemistry was performed by using a PBS solution containing 1.5% normal goat serum and 0.25% Triton X-100 for all procedures. The washing steps were done with PBS. The sections were incubated overnight (ON) at 4°C with selected antibodies, followed by incubation at 4°C ON with donkey secondary antibodies (Jackson ImmunoResearch Laboratories).

For cell counting and *post hoc* examination of marker expression, sections were stained using rat anti-GFP, mouse anti-Reelin (1:500, MBL, D223-3), rabbit anti-dsRed (Abcam, ab62341), rabbit anti-VIP (1:1,000, Immunostar, 20077), Gt-PV (1:500, Swant:PVG214), and rat anti-SST (1:500, Millipore). For the analysis of nuclear localization of NFATc4 protein, rabbit NFATc4 (Abcam, ab62613, 1:500) was used.

Neuronal Morphology Analysis

Neuronal morphology was obtained either by using the *in utero* electroporation method or by using whole-cell physiology to fill the cells with biotin. Successful targeting of the desired Reelin- and VIP-expressing populations in all of our experiments was confirmed through *post hoc* examination of marker expression. The morphology of neurons obtained from the confocal stacks was reconstructed using Neurolucida (4-μm interval, 250-μm-thick sections). Morphometric analysis was done using Neurolucida Explorer for both the axonal and dendritic length and branching.

Electrophysiology and Analysis

Whole-cell patch-clamp electrophysiological recordings were performed on EGFP+ and EGFP-negative cells of layers I–III in acute brain slices prepared from P16-P21 animals. Briefly, animals were decapitated, and the brain was dissected out and transferred to physiological Ringer's solution (artificial cerebrospinal fluid [ACSF]) cooled to 4°C, of the following composition: 125 mM NaCl, 2.5 mM KCl, 25 mM $NaHCO_3$, 1.25 mM NaH_2PO_4, 1 mM $MgCl_2$, 2 mM $CaCl_2$, and 20 mM glucose. The brain was then glued to a stage, and slices of 250-300 μm were cut using a vibratome (Vibratome 3000 EP). The slices were allowed to recover in recording ACSF at room temperature for at least 45 min before recording. Acute slices were then placed in a recording chamber mounted on the stage of an upright microscope (Axioscope, Zeiss, Germany) equipped with immersion differential interference contrast objectives (5× and 40×) coupled to an infrared camera system (Zeiss), superfused at a rate of 1-2 mL/min with oxygenated recording ACSF, and maintained at a temperature of 31 °C. An EGFP filter was used to visualize the fluorescent interneurons in epifluorescence.

Patch electrodes were made from borosilicate glass (Harvard Apparatus) and had a resistance of 4–8 megaohm (MΩ). For both intrinsic electrophysiological properties and sEPSC recordings, the patch pipettes were filled with a solution containing the following: 128 mM potassium gluconate, 4 mM NaCl, 0.3 mM sodium guanosine triphosphate (Na-GTP), 5 mM Mg-ATP, 0.0001 mM $CaCl_2$, and 10 mM 4-(2-hydroxyethyl)-1-piperazineethanesulfonic acid (HEPES). For recording sIPSCs, the patch pipettes were filled with a solution containing the following: 65 mM KCl, 65 mM K-gluconate, 4 mM NaCl, 0.3 mM Na-GTP, 5 mM Mg-ATP, 0.0001 mM $CaCl_2$, and 10 mM HEPES.

α-amino-3-hydroxy-5-methyl-4-isoxazolepropionic acid receptor (AMPAR)-mediated currents were recorded at −70 mV with no drugs in the bath, whereas gamma-aminobutyric acid receptor ($GABA_AR$)-mediated currents were recorded at −70 mV in the presence of 3 μM kynurenic acid. Experiments were performed in current-clamp and voltage-clamp modes using the Axopatch 200B amplifier (Molecular Devices). sEPSCs and sIPSCs were recorded in multiple epochs of 2–4 min at holding potential (V_h) = −70 mV with a sampling rate of 10 kHz and filtered online at 3 kHz. The recorded events were analyzed using Minianalysis software (Synaptosoft, Decatur, GA, USA) or Clampfit. The area was measured as an absolute value of the integral of the synaptic current. The decay time was calculated by fitting the average trace with a single exponential. Access resistance was always monitored to ensure the stability of recording conditions. Cells were accepted for analysis only when

the initial series resistance was less than or equal to 30 MΩ and did not change by more than 20% throughout the recording period. No compensation was made for access resistance, and no correction was made for the junction potential between the pipette and the ACSF. Passive and active membrane properties were recorded in current-clamp mode by applying a series of sub- and suprathreshold current steps. The analysis was done in Clampfit. The resting membrane potential was ascertained in current-clamp mode right after rupturing the patch by applying zero current. All values presented in the manuscript are average ± SEM, and all comparisons were done using a Mann-Whitney test.

Cell Counting

20-μm-thick coronal sections were used for all of our analyses. Brains were manually cut perpendicular to the horizontal plane, using the cerebellum as a reference for mounting. The angle of cut was confirmed by the co-emergence of the caudoputamen and anterior commissure. For counting the CGE-derived cortical interneuron population, we utilized the 5Ht3aR^{eGFP} transgenic line (Figure 1). We analyzed brain sections between two well-defined anatomical landmarks, beginning with the appearance of the claustrum (at the most anterior part of the striatum) until the disappearance of the splenium. This allowed us to analyze equivalent regions and account for changes in the whole-brain volume with age. Specifically, we found that the observed changes in cell density cannot be accounted for simply by the increase in brain size across these two ages. The specific methods involved in counting the number of GFP+ neurons involved the collection and analysis of every tenth section within the cortical region defined and quantitating the number of GFP+ neurons across the medial-lateral extent of these sections (Figure S1A). To calculate total GFP numbers, we used the fractionation method by using the following formula in our final analysis:

$$N = \sum Q^{-} \bullet \frac{1}{asf} \bullet \frac{1}{ssf}, \quad \text{Equation 1}$$

where, Q^{-} is particles counted, asf is the area sampling fraction (1 in our experimental design), and ssf is the section sampling fraction (10 in our experimental design).

In experiments using AAV injections and FK506 treatment, we restricted our analysis to the cortical region between two anatomical landmarks as injections were focally targeted: beginning with the appearance of the lateral ventricle until the disappearance of the caudoputamen. Brains used for quantification of cell density were manually cut perpendicular to the horizontal plane; the angle of cut was confirmed as described above.

The coordinates for virus injections (and FK506) were taken from the Atlas of the Developing Mouse Brain (Paxinos, 2007). The injections were made at positions x = 1.5 and y = 3 mm from the bregma. 350 nL of virus was injected into the cortex at a cortical depth of 150 μm.

For quantifying interneuronal population size upon AAV injections, we analyzed 3 slices per hemisphere for each animal: one section containing the injection core and an alternate

section either anterior or posterior to the core. We imaged each section using a 10× lens on a Zeiss confocal microscope and generated z stacks with 4-μm intervals. We then performed a maximum projection of these z stacks and overlaid a standardized counting frame (250/550 pixel or 156/350 μm area) encompassing the cortical area with viral infection. We calculated the cell density for each section and then took an average of those 3 sections. A similar analysis was done for each brain, and the values obtained were averaged to calculate the mean and the SEM.

Importantly, we found, with either control or experimental AAV injections, that the infection site uniformly labeled the entire quantitated area, ensuring that the level of injection did not affect the experimental outcome. Within this area, we calculated the density of interneurons by counting the number of GFP+ neurons and different immunomarkers that labeled interneuron subtypes; for example, Reelin, VIP, PV, and SST.

To account for the variability in the site of injection and facilitate comparisons of cell numbers across samples, we normalized our cell density counts to the equivalent region on the contralateral site. We normalized the cell density as described below (Equation 1). The percentage of change in cell density = (cell count on the injected side) × (100)/(cell count on the uninjected site). A minimum of three brains was analyzed per age (n = 3) unless stated otherwise, and averages are shown with the SEM.

For measuring the cell density in the conditional KOs and aged-matched controls, 20-μm-thick tissue sections were used for analysis. The stringency in the angle of cut was maintained as described above. We restricted our analysis to the somatosensory cortex (except for Figure S7F, where, along with the somatosensory cortex, we also analyzed the motor and visual cortex). The appearance of the hippocampus was used to identify the reference section for the somatosensory cortex. We then selected an alternate section anterior or posterior to the identified section to obtain a total of 3 sections per brain. Each section was imaged as previously mentioned. Similarly, we identified the motor cortex by the appearance of the body of the caudoputamen and the visual cortex by the disappearance of the lateral ventricle as a reference landmark. Again, 3 alternating sections were chosen for each cortical area per brain along these referred landmarks. The cell density of GFP+ neurons was counted by electronically superimposing a 250 × 550 pixel area on the region of interest. We determined the cell density in the somatosensory cortex by taking the average of 3 sections per animal. A similar analysis was done for each brain, and the values obtained were averaged to calculate the mean and the SEM. For quantification of the interneuron subtypes, we calculated the density of each subtype by co-immunostaining of immunomarkers like Reelin and VIP with GFP. A similar analysis was done for cleaved caspase-3 staining.

Statistical Analysis

All statistical analyses were performed using unpaired t test or Mann-Whitney *U* test. For all electrophysiology data analyses, the nonparametric Mann-Whitney test was chosen because the number of values compared was not high enough to justify a normality test and usage of the unpaired t test. All values represent mean values ± SEM. For all other data, normality and an estimate of variance were formally tested with GraphPad Prism. For the tamoxifen-

induced experiments, a paired t test was used to take into account the day-to-day variability between different litters injected with tamoxifen. The analyses of the integrated density of NFATc4 immunostaining under different conditions were blinded to genotype. For the statistics of cultured neurons, ANOVA was used to determine significance. No statistical methods were used to predetermine sample sizes, but our sample sizes were similar to those reported in previous publications.

Supplementary Material

Refer to Web version on PubMed Central for supplementary material.

Acknowledgments

We are grateful to Richard W. Tsien and Robert Machold for comments on the manuscript. We also thank Latika Khatri for helping us with western blots. This work was supported by NIH grants R01-NS081297, R01-MH071679, and P01-NS074972 and generous support from the Simons Foundation (grant no. 274578). Work in the Alvarez-Buylla laboratory is supported by NIH grants K08NS091537-01A1 and R01-EY025174 and a generous gift from the John G. Bowes Research Fund. A.A.-B. is the Heather and Melanie Muss Endowed Chair and Professor of Neurological Surgery at UCSF.

References

Allène C, Cattani A, Ackman JB, Bonifazi P, Aniksztejn L, Ben-Ari Y, Cossart R. Sequential generation of two distinct synapse-driven network patterns in developing neocortex. J Neurosci. 2008; 28:12851–12863. [PubMed: 19036979]

Alvarez-Buylla A, Kirn JR, Nottebohm F. Birth of projection neurons in adult avian brain may be related to perceptual or motor learning. Science. 1990; 249:1444–1446. [PubMed: 1698312]

Bando Y, Irie K, Shimomura T, Umeshima H, Kushida Y, Kengaku M, Fujiyoshi Y, Hirano T, Tagawa Y. Control of Spontaneous Ca2+ Transients Is Critical for Neuronal Maturation in the Developing Neocortex. Cereb Cortex. 2016; 26:106–117. [PubMed: 25112282]

Batista-Brito R, Machold R, Klein C, Fishell G. Gene expression in cortical interneuron precursors is prescient of their mature function. Cereb Cortex. 2008; 18:2306–2317. [PubMed: 18250082]

Baumgä rtel K, Mansuy IM. Neural functions of calcineurin in synaptic plasticity and memory. Learn Mem. 2012; 19:375–384. [PubMed: 22904368]

Beals CR, Clipstone NA, Ho SN, Crabtree GR. Nuclear localization of NF-ATc by a calcineurin-dependent, cyclosporin-sensitive intramolecular interaction. Genes Dev. 1997; 11:824–834. [PubMed: 9106655]

Bean BP. Classes of calcium channels in vertebrate cells. Annu Rev Physiol. 1989; 51:367–384. [PubMed: 2540697]

Beattie EC, Carroll RC, Yu X, Morishita W, Yasuda H, von Zastrow M, Malenka RC. Regulation of AMPA receptor endocytosis by a signaling mechanism shared with LTD. Nat Neurosci. 2000; 3:1291–1300. [PubMed: 11100150]

Blanquie O, Yang JW, Kilb W, Sharopov S, Sinning A, Luhmann HJ. Electrical activity controls area-specific expression of neuronal apoptosis in the mouse developing cerebral cortex. eLife. 2017; 6:e27696. [PubMed: 28826501]

Bonci A, Grillner P, Mercuri NB, Bernardi G. L-Type calcium channels mediate a slow excitatory synaptic transmission in rat midbrain dopaminergic neurons. J Neurosci. 1998; 18:6693–6703. [PubMed: 9712641]

Brosenitsch TA, Katz DM. Physiological patterns of electrical stimulation can induce neuronal gene expression by activating N-type calcium channels. J Neurosci. 2001; 21:2571–2579. [PubMed: 11306610]

Butt SJB, Fuccillo M, Nery S, Noctor S, Kriegstein A, Corbin JG, Fishell G. The temporal and spatial origins of cortical interneurons predict their physiological subtype. Neuron. 2005; 48:591–604. [PubMed: 16301176]

Cameron S, Clark SG, McDermott JB, Aamodt E, Horvitz HR. PAG-3, a Zn-finger transcription factor, determines neuroblast fate in C. elegans. Development. 2002; 129:1763–1774. [PubMed: 11923211]

Chang CD, Mukai H, Kuno T, Tanaka C. cDNA cloning of an alternatively spliced isoform of the regulatory subunit of Ca2+/calmodulin-dependent protein phosphatase (calcineurin B α 2). Biochim Biophys Acta. 1994; 1217:174–180. [PubMed: 8110831]

Clayton EL, Anggono V, Smillie KJ, Chau N, Robinson PJ, Cousin MA. The phospho-dependent dynamin-syndapin interaction triggers activity-dependent bulk endocytosis of synaptic vesicles. J Neurosci. 2009; 29:7706–7717. [PubMed: 19535582]

Clipstone NA, Crabtree GR. Identification of calcineurin as a key signalling enzyme in T-lymphocyte activation. Nature. 1992; 357:695–697. [PubMed: 1377362]

Close J, Xu H, De Marco García N, Batista-Brito R, Rossignol E, Rudy B, Fishell G. Satb1 is an activity-modulated transcription factor required for the terminal differentiation and connectivity of medial ganglionic eminence-derived cortical interneurons. J Neurosci. 2012; 32:17690–17705. [PubMed: 23223290]

Conradt B, Horvitz HR. The C. elegans protein EGL-1 is required for programmed cell death and interacts with the Bcl-2-like protein CED-9. Cell. 1998; 93:519–529. [PubMed: 9604928]

Daval JL, Nakajima T, Gleiter CH, Post RM, Marangos PJ. Mouse brain c-fos mRNA distribution following a single electroconvulsive shock. J Neurochem. 1989; 52:1954–1957. [PubMed: 2723651]

De Marco Garcia NV, Fishell G. Subtype-selective electroporation of cortical interneurons. J Vis Exp. 2014; 90:e51518.

De Marco García NV, Karayannis T, Fishell G. Neuronal activity is required for the development of specific cortical interneuron subtypes. Nature. 2011; 472:351–355. [PubMed: 21460837]

De Marco García NV, Priya R, Tuncdemir SN, Fishell G, Karayannis T. Sensory inputs control the integration of neurogliaform interneurons into cortical circuits. Nat Neurosci. 2015; 18:393–401. [PubMed: 25664912]

Dehorter N, Ciceri G, Bartolini G, Lim L, del Pino I, Marí n O. Tuning of fast-spiking interneuron properties by an activity-dependent transcriptional switch. Science. 2015; 349:1216–1220. [PubMed: 26359400]

Dexana M, Neves G, Rabinowitz A, Kemlo S, Liodis P, Burrone J, Pachnis V. Modulation of apoptosis controls inhibitory interneuron number in the cortex. Cell Reports. 2018; 20:1710–1721. this issue.

Doetsch F, Caillé I, Lim DA, García-Verdugo JM, Alvarez-Buylla A. Subventricular zone astrocytes are neural stem cells in the adult mammalian brain. Cell. 1999; 97:703–716. [PubMed: 10380923]

Dolmetsch RE, Xu K, Lewis RS. Calcium oscillations increase the efficiency and specificity of gene expression. Nature. 1998; 392:933–936. [PubMed: 9582075]

Evans GJO, Cousin MA. Activity-dependent control of slow synaptic vesicle endocytosis by cyclin-dependent kinase 5. J Neurosci. 2007; 27:401–411. [PubMed: 17215401]

Flanagan WM, Corthésy B, Bram RJ, Crabtree GR. Nuclear association of a T-cell transcription factor blocked by FK-506 and cyclosporin A. Nature. 1991; 352:803–807. [PubMed: 1715516]

Fu Y, Tucciarone JM, Espinosa JS, Sheng N, Darcy DP, Nicoll RA, Huang ZJ, Stryker MP. A cortical circuit for gain control by behavioral state. Cell. 2014; 156:1139–1152. [PubMed: 24630718]

Gage FH. Mammalian neural stem cells. Science. 2000; 287:1433–1438. [PubMed: 10688783]

Gage FH, Temple S. Neural stem cells: generating and regenerating the brain. Neuron. 2013; 80:588–601. [PubMed: 24183012]

Ghosh A, Greenberg ME. Calcium signaling in neurons: molecular mechanisms and cellular consequences. Science. 1995; 268:239–247. [PubMed: 7716515]

Ghosh A, Carnahan J, Greenberg ME. Requirement for BDNF in activity-dependent survival of cortical neurons. Science. 1994; 263:1618–1623. [PubMed: 7907431]

Graef IA, Mermelstein PG, Stankunas K, Neilson JR, Deisseroth K, Tsien RW, Crabtree GR. L-type calcium channels and GSK-3 regulate the activity of NF-ATc4 in hippocampal neurons. Nature. 1999; 401:703–708. [PubMed: 10537109]

Greenberg ME, Ziff EB, Greene LA. Stimulation of neuronal acetylcholine receptors induces rapid gene transcription. Science. 1986; 234:80–83. [PubMed: 3749894]

Guo JU, Su Y, Zhong C, Ming GL, Song H. Hydroxylation of 5-methylcytosine by TET1 promotes active DNA demethylation in the adult brain. Cell. 2011; 145:423–434. [PubMed: 21496894]

Haider B, Duque A, Hasenstaub AR, McCormick DA. Neocortical network activity in vivo is generated through a dynamic balance of excitation and inhibition. J Neurosci. 2006; 26:4535–4545. [PubMed: 16641233]

Haider B, Häusser M, Carandini M. Inhibition dominates sensory responses in the awake cortex. Nature. 2013; 493:97–100. [PubMed: 23172139]

Hempel CM, Sugino K, Nelson SB. A manual method for the purification of fluorescently labeled neurons from the mammalian brain. Nat Protoc. 2007; 2:2924–2929. [PubMed: 18007629]

Henderson CE, Phillips HS, Pollock RA, Davies AM, Lemeulle C, Armanini M, Simmons L, Moffet B, Vandlen RA, Simpson LC, et al. GDNF: a potent survival factor for motoneurons present in peripheral nerve and muscle. Science. 1994; 266:1062–1064. corrected to Simmons L. [PubMed: 7973664]

Horvitz HR. Worms, life, and death (Nobel lecture). ChemBioChem. 2003; 4:697–711. [PubMed: 12898619]

Iijima T, Wu K, Witte H, Hanno-Iijima Y, Glatter T, Richard S, Scheiffele P. SAM68 regulates neuronal activity-dependent alternative splicing of neurexin-1. Cell. 2011; 147:1601–1614. [PubMed: 22196734]

Jin G, Omori N, Li F, Sato K, Nagano I, Manabe Y, Shoji M, Abe K. Activation of cell-survival signal Akt by GDNF in normal rat brain. Brain Res. 2002; 958:429–433. [PubMed: 12470880]

Kepecs A, Fishell G. Interneuron cell types are fit to function. Nature. 2014; 505:318–326. [PubMed: 24429630]

Khazipov R, Sirota A, Leinekugel X, Holmes GL, Ben-Ari Y, Buzsáki G. Early motor activity drives spindle bursts in the developing somatosensory cortex. Nature. 2004; 432:758–761. [PubMed: 15592414]

Kim S, Ziff EB. Calcineurin mediates synaptic scaling via synaptic trafficking of Ca2+-permeable AMPA receptors. PLoS Biol. 2014; 12:e1001900. [PubMed: 24983627]

Klee CB, Crouch TH, Krinks MH. Calcineurin: a calcium- and calmodulin-binding protein of the nervous system. Proc Natl Acad Sci USA. 1979; 76:6270–6273. [PubMed: 293720]

Kokaia Z, Bengzon J, Metsis M, Kokaia M, Persson H, Lindvall O. Coexpression of neurotrophins and their receptors in neurons of the central nervous system. Proc Natl Acad Sci USA. 1993; 90:6711–6715. [PubMed: 8341689]

Lee S, Hjerling-Leffler J, Zagha E, Fishell G, Rudy B. The largest group of superficial neocortical GABAergic interneurons expresses ionotropic serotonin receptors. J Neurosci. 2010; 30:16796–16808. [PubMed: 21159951]

Lee S, Kruglikov I, Huang ZJ, Fishell G, Rudy B. A disinhibitory circuit mediates motor integration in the somatosensory cortex. Nat Neurosci. 2013; 16:1662–1670. [PubMed: 24097044]

Levi-Montalcini R. The nerve growth factor 35years later. Science. 1987; 237:1154–1162. [PubMed: 3306916]

Lieberman DN, Mody I. Regulation of NMDA channel function by endogenous Ca(2+)-dependent phosphatase. Nature. 1994; 369:235–239. [PubMed: 7514273]

Lin LF, Doherty DH, Lile JD, Bektesh S, Collins F. GDNF: a glial cell line-derived neurotrophic factor for midbrain dopaminergic neurons. Science. 1993; 260:1130–1132. [PubMed: 8493557]

Lin CW, Sim S, Ainsworth A, Okada M, Kelsch W, Lois C. Genetically increased cell-intrinsic excitability enhances neuronal integration into adult brain circuits. Neuron. 2010; 65:32–39. [PubMed: 20152111]

Lodato S, Rouaux C, Quast KB, Jantrachotechatchawan C, Studer M, Hensch TK, Arlotta P. Excitatory projection neuron subtypes control the distribution of local inhibitory interneurons in the cerebral cortex. Neuron. 2011; 69:763–779. [PubMed: 21338885]

Lois C, García-Verdugo JM, Alvarez-Buylla A. Chain migration of neuronal precursors. Science. 1996; 271:978–981. [PubMed: 8584933]

Mardinly AR, Spiegel I, Patrizi A, Centofante E, Bazinet JE, Tzeng CP, Mandel-Brehm C, Harmin DA, Adesnik H, Fagiolini M, Greenberg ME. Sensory experience regulates cortical inhibition by inducing IGF1 in VIP neurons. Nature. 2016; 531:371–375. [PubMed: 26958833]

McKay SE, Garner A, Caldero J, Tucker RP, Large T, Oppenheim RW. The expression of trkB and p75 and the role of BDNF in the developing neuromuscular system of the chick embryo. Development. 1996; 122:715–724. [PubMed: 8625822]

Mermelstein PG, Bito H, Deisseroth K, Tsien RW. Critical dependence of cAMP response element-binding protein phosphorylation on L-type calcium channels supports a selective response to EPSPs in preference to action potentials. J Neurosci. 2000; 20:266–273. [PubMed: 10627604]

Miller FD, Kaplan DR. Neurotrophin signalling pathways regulating neuronal apoptosis. Cell Mol Life Sci. 2001; 58:1045–1053. [PubMed: 11529497]

Miyoshi G, Butt SJB, Takebayashi H, Fishell G. Physiologically distinct temporal cohorts of cortical interneurons arise from telencephalic Olig2-expressing precursors. J Neurosci. 2007; 27:7786–7798. [PubMed: 17634372]

Miyoshi G, Hjerling-Leffler J, Karayannis T, Sousa VH, Butt SJB, Bat-tiste J, Johnson JE, Machold RP, Fishell G. Genetic fate mapping reveals that the caudal ganglionic eminence produces a large and diverse population of superficial cortical interneurons. J Neurosci. 2010; 30:1582–1594. [PubMed: 20130169]

Oppenheim RW. The neurotrophic theory and naturally occurring motoneuron death. Trends Neurosci. 1989; 12:252–255. [PubMed: 2475935]

Oppenheim RW, Prevette D, Haverkamp LJ, Houenou L, Yin QW, McManaman J. Biological studies of a putative avian muscle-derived neurotrophic factor that prevents naturally occurring motoneuron death in vivo. J Neurobiol. 1993; 24:1065–1079. [PubMed: 8409968]

Paxinos G. Atlas of the Developing Mouse Brain. Academic Press; 2007.

Pi HJ, Hangya B, Kvitsiani D, Sanders JI, Huang ZJ, Kepecs A. Cortical interneurons that specialize in disinhibitory control. Nature. 2013; 503:521–524. [PubMed: 24097352]

Polleux F, Whitford KL, Dijkhuizen PA, Vitalis T, Ghosh A. Control of cortical interneuron migration by neurotrophins and PI3-kinase signaling. Development. 2002; 129:3147–3160. [PubMed: 12070090]

Polleux F, Ince-Dunn G, Ghosh A. Transcriptional regulation of vertebrate axon guidance and synapse formation. Nat Rev Neurosci. 2007; 8:331–340. [PubMed: 17453014]

Pouille F, Scanziani M. Enforcement of temporal fidelity in pyramidal cells by somatic feed-forward inhibition. Science. 2001; 293:1159–1163. [PubMed: 11498596]

Riccio A, Ahn S, Davenport CM, Blendy JA, Ginty DD. Mediation by a CREB family transcription factor of NGF-dependent survival of sympathetic neurons. Science. 1999; 286:2358–2361. [PubMed: 10600750]

Sahay A, Hen R. Adult hippocampal neurogenesis in depression. Nat Neurosci. 2007; 10:1110–1115. [PubMed: 17726477]

Sík A, Hájos N, Gulácsi A, Mody I, Freund TF. The absence of a major Ca2+ signaling pathway in GABAergic neurons of the hippocampus. Proc Natl Acad Sci USA. 1998; 95:3245–3250. [PubMed: 9501248]

Song H, Stevens CF, Gage FH. Astroglia induce neurogenesis from adult neural stem cells. Nature. 2002; 417:39–44. [PubMed: 11986659]

Southwell DG, Paredes MF, Galvao RP, Jones DL, Froemke RC, Sebe JY, Alfaro-Cervello C, Tang Y, Garcia-Verdugo JM, Rubenstein JL, et al. Intrinsically determined cell death of developing cortical interneurons. Nature. 2012; 491:109–113. [PubMed: 23041929]

Sulston JE, White JG. Regulation and cell autonomy during postembryonic development of Caenorhabditis elegans. Dev Biol. 1980; 78:577–597. [PubMed: 7190941]

Sussman MA, Lim HW, Gude N, Taigen T, Olson EN, Robbins J, Colbert MC, Gualberto A, Wieczorek DF, Molkentin JD. Prevention of cardiac hypertrophy in mice by calcineurin inhibition. Science. 1998; 281:1690–1693. [PubMed: 9733519]

Tsien RW, Lipscombe D, Madison DV, Bley KR, Fox AP. Multiple types of neuronal calcium channels and their selective modulation. Trends Neurosci. 1988; 11:431–438. [PubMed: 2469160]

Tuncdemir SN, Fishell G, Batista-Brito R. miRNAs are Essential for the Survival and Maturation of Cortical Interneurons. Cereb Cortex. 2015; 25:1842–1857. [PubMed: 24451661]

Ueki K, Muramatsu T, Kincaid RL. Structure and expression of two isoforms of the murine calmodulin-dependent protein phosphatase regulatory subunit (calcineurin B). Biochem Biophys Res Commun. 1992; 187:537–543. [PubMed: 1325794]

Wehr M, Zador AM. Balanced inhibition underlies tuning and sharpens spike timing in auditory cortex. Nature. 2003; 426:442–446. [PubMed: 14647382]

West AE, Greenberg ME. Neuronal activity-regulated gene transcription in synapse development and cognitive function. Cold Spring Harb Perspect Biol. 2011; 3:a005744. [PubMed: 21555405]

Wheeler DG, Groth RD, Ma H, Barrett CF, Owen SF, Safa P, Tsien RW. Ca(V)1 and Ca(V)2 channels engage distinct modes of Ca(2+) signaling to control CREB-dependent gene expression. Cell. 2012; 149:1112–1124. [PubMed: 22632974]

Xu Q, Cobos I, De La Cruz E, Rubenstein JL, Anderson SA. Origins of cortical interneuron subtypes. J Neurosci. 2004; 24:2612–2622. [PubMed: 15028753]

Yasuda H, Barth AL, Stellwagen D, Malenka RC. A developmental switch in the signaling cascades for LTP induction. Nat Neurosci. 2003; 6:15–16. [PubMed: 12469130]

Yu CR, Power J, Barnea G, O'Donnell S, Brown HEV, Osborne J, Axel R, Gogos JA. Spontaneous neural activity is required for the establishment and maintenance of the olfactory sensory map. Neuron. 2004; 42:553–566. [PubMed: 15157418]

Yu M, Xi Y, Pollack J, Debiais-Thibaud M, Macdonald RB, Ekker M. Activity of dlx5a/dlx6a regulatory elements during zebrafish GABAergic neuron development. Int J Dev Neurosci. 2011; 29:681–691. [PubMed: 21723936]

Highlights

- Neuronal activity reduces cell death in most cortical interneuron subtypes
- Unlike other interneurons, apoptosis in VIP interneurons is not activity-dependent
- Calcineurin signaling promotes interneuron survival
- Calcineurin acts as a dual regulator of both maturation and cell death

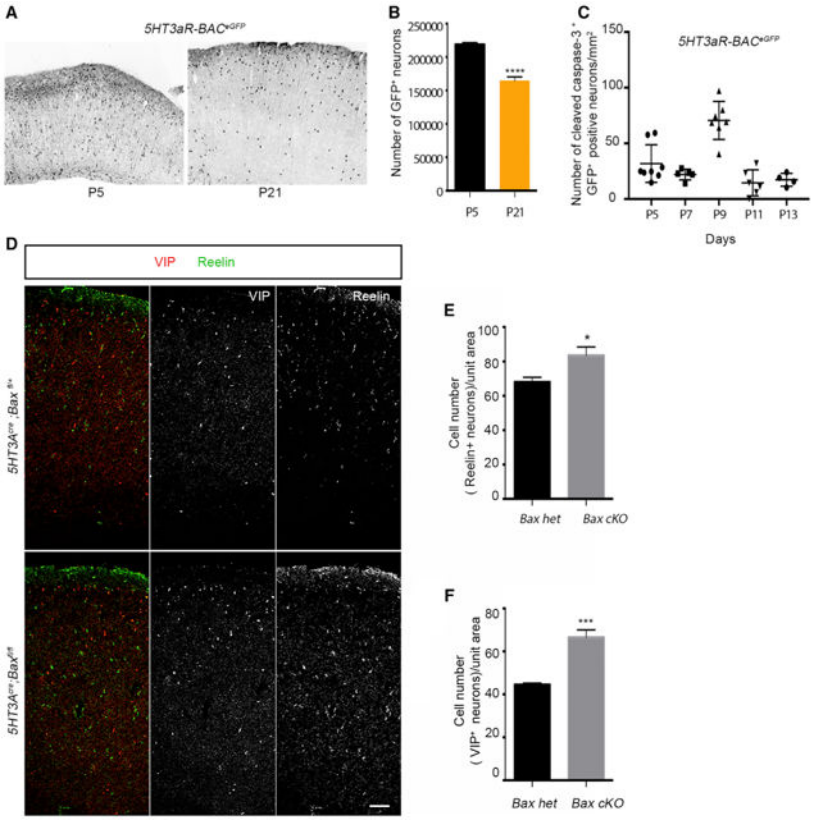

Figure 1. Cell Death in CGE-Derived Interneurons Is Bax-Mediated

(A) Representative image of coronal sections from 5HT3aR-BACeGFP cortex at P5 and P21.

(B) Quantification of the number of EGFP+ neurons in the cortex at P21 compared with P5 ($n \geq 3$, $p = < 0.0001$).

(C) Density analysis of cleaved caspase-3+, GFP+ interneurons at different postnatal time points. ANOVA, statistical difference, $p < 0.0001$, $n \geq 3$.

(D) Representative sections showing the density of Reelin- and VIP-expressing interneurons in control and Bax cKOs. Scale bar, 100 μm.

(E) Quantification reveals an increase in density of Reelin+ interneurons in Bax cKOs compared with the control. $n \geq 3$; $p = 0.01412$.

(F) Quantification reveals an increase in density of VIP+ interneurons in Bax cKOs compared with the control. $n \geq 3$; $p = 0.001$.

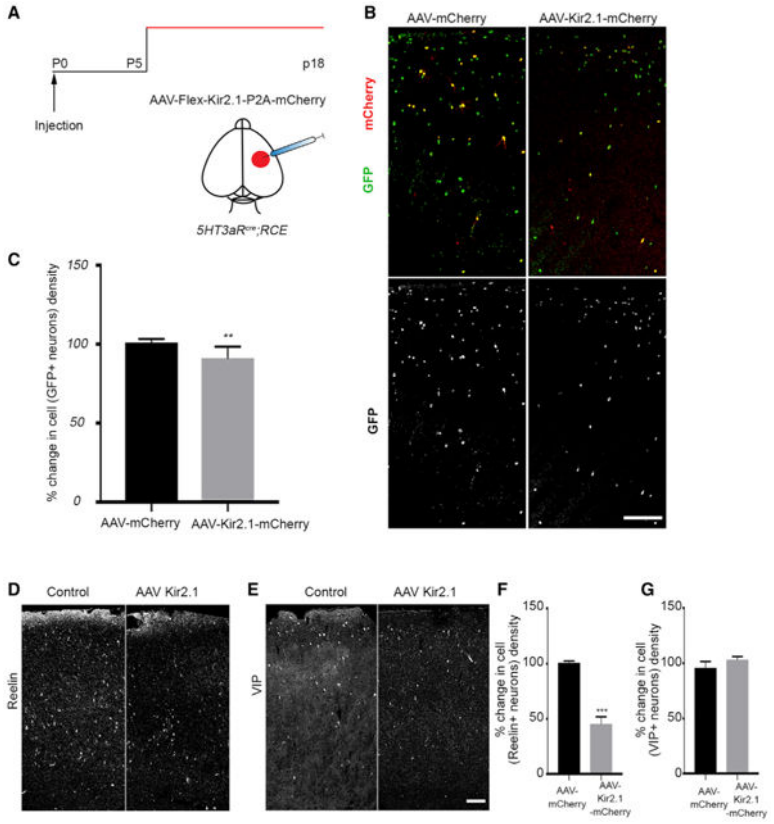

Figure 2. Activity Regulates Cell Death of Specific CGE-Derived Interneuron Subtypes in the Developing Cortex

(A) Schematic representation of the experimental strategy.

(B) Representative section of the cortex with AAV injections. Left: a coronal section from a 5HT3aR^{cre};RCE brain injected with AAV-flex-mCherry. Right: 5HT3aR^{cre};RCE brain section injected with AAV-flex-Kir2.1-P2A-mCherry.

(C) Quantification of the percent change in cell density of GFP+ interneurons in the AAV-Kir2.1-mCherry-injected hemisphere compared with the control ($p = 0.0057$, $n \geq 3$).

(D) Representative images showing coronal sections from 5HT3aR^{cre};RCE brains injected with control (left) and AAV-flex-Kir2.1-P2A-mCherry virus (right) immunostained for Reelin.

(E) Representative images showing coronal sections from 5HT3aR^{cre};RCE brains injected with control (left) and AAV-flex-Kir2.1-P2A-mCherry virus (right)immunostained for VIP.

(F) Quantification of the percent change in cell density of Reelin+ interneurons in AAV-Kir2.1-mCherry-injected brain compared with the control (mean ± SEM, $p = 0.0.006$, unpaired t test, $n \geq 3$).

(G) Quantification of the percent change in cell density of VIP+ interneurons in AAV-Kir2.1-mCherry-injected brain compared with the control (mean ± SEM, $p = 0.1135$, unpaired t test, $n \geq 3$). Scale bars, 100 μm. See also Figures S2 and S3.

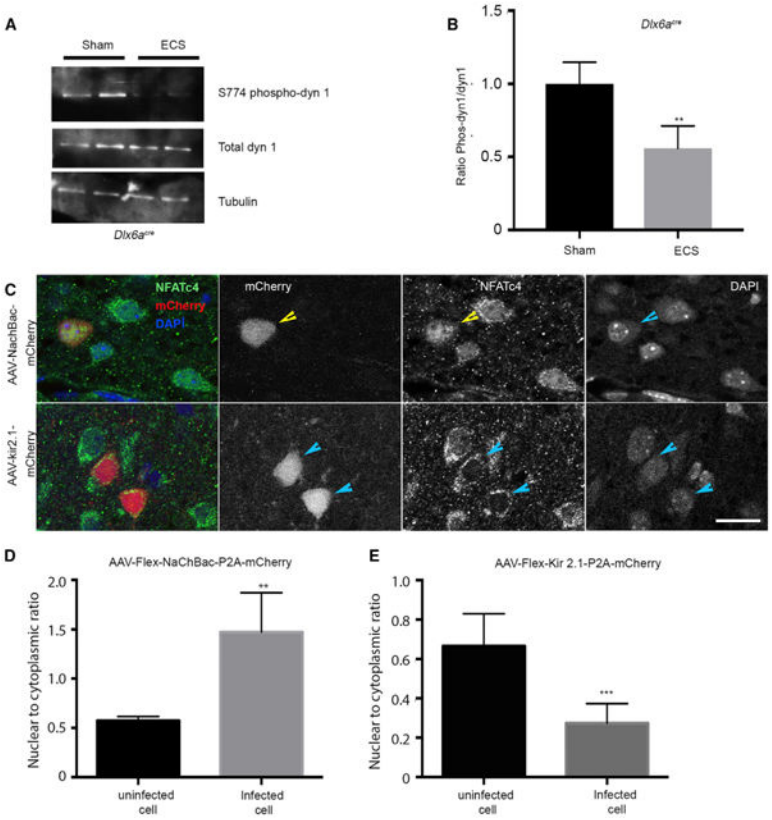

Figure 3. Canonical CaN Targets Are Activated by ECS

(A) Western blot of interneuron lysates, sorted by FACS from ECS- or sham-treated animals (duplicates are shown) and probed for total dynamin, phospho-S774 dynamin 1, and tubulin.

(B) Quantification of phospho-dynamin 1 reveals a reduction in the levels, 3 hr after an ECS treatment was applied to P7 mice compared with sham-treated littermates. n = 4, p = 0.0178 (unpaired t test).

(C) Representative image showing cellular localization of NFATc4 upon NaChbac (top) and Kir2.1 overexpression (bottom).

(D) Quantification of the nuclear-to-cytoplasmic ratio of integrated density of NFATc4 immunolabeling shows an increase in NaChbac-expressing cells. n = 3, p = 0.0042 (unpaired t test).

(E) Quantification of the nuclear-to-cytoplasmic ratio of NFATc4 expression in Kir2.1-mCherry-injected compared with uninfected cells. n = 3, p = 0.0008 (unpaired t test). Scale bar, 10 μm. See also Figure S4.

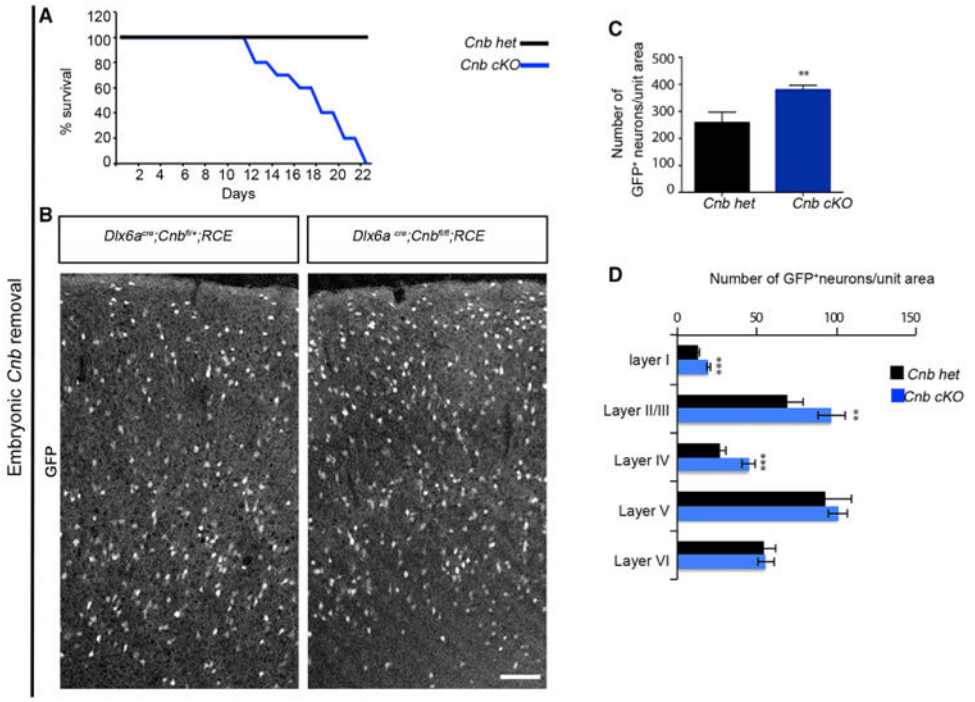

Figure 4. CaN Regulates Cell Death within Interneurons during Development

(A) Survival percent indicates increased mortality in animals lacking the Cnb gene in interneurons compared with their control littermates.

(B) Representative image of coronal sections showing the distribution of GFP+ interneurons upon conditional removal of Cnb using a Dlx6acre driver line. Animals were sacrificed between P18–P21.

(C) Quantification of GFP+ interneurons in the cortex shows a significant increase in the density of Cnb cKO compared with controls. n = 5, p = 0.0010, paired t test.

(D) Layer distribution of GFP+ interneurons shows an increase in density in superficial layers without affecting deeper layers upon Cnb removal. Layer I, p = 0.0030; layers II/III, p = 0.050; layer IV, p = 0.013, laver V, p = 0.493; layer VI, p = 0.890. Scale bar, 100 μm. See also Figure S5.

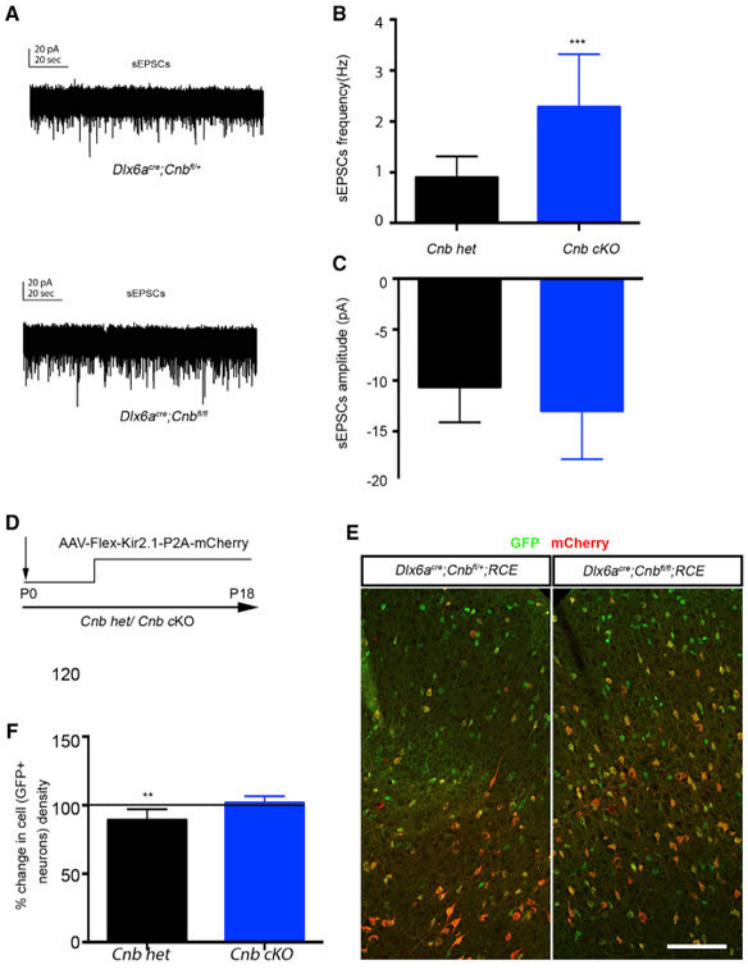

Figure 5. Increases in the Number of Inter-neurons in Embryonic Cnb cKOs Are Not Due to an Increase in Neuronal Activity

(A) Representative traces of sEPSCs recorded from layer I interneurons *in vitro* (top, control;bottom, Cnb cKO).

(B) Quantification of amplitude of sEPSCs. cKO of Cnb results in an increase in frequency. n ≥ 3, number of cells recorded for control = 16 and mutant = 11. Mann-Whitney test, p = 0.0009.

(C) Quantification of frequency of sEPSCs. cKO of Cnb results in no change in amplitude, n ≥ 3, Mann-Whitney test, p = 0.0974.

(D) Schematic of the experimental design.

(E) Representative image of coronal sections fromDlx6a^{cre};Cnbfl/fl;RCE mice injected with AAV-flex-Kir2.1-mCherry.

(F) Quantification of percent change in density of GFP+ neurons in Cnb cKO and control. n ≥ 3, unpaired t test, p = 0.0006. Scale bar, 100 μm.

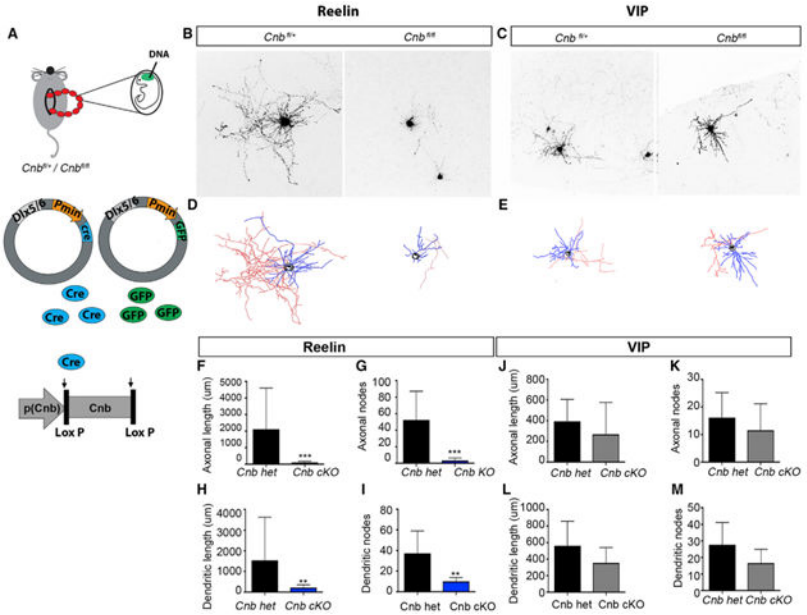

Figure 6. Removal of CaN Has No Effect on the Maturation of VIP-Expressing Interneurons

(A) Schematic representation of the experimental strategy.

(B) Representative image of Reelin+ interneurons in CnB heterozygous (het) and CnB cKO animals.

(C) Representative image of VIP+ neurons in CnB het and CnB cKO mice.

(D) Reconstructed Neurolucida drawing of Reelin+ interneurons.

(E) Reconstructed Neurolucida drawing of VIP+ interneurons. Red denotes axonal reconstruction, blue denotes dendrites, and black indicates somata.

(F–I) Morphometric analysis of Reelin+ interneurons shows a reduction in both axonal and dendritic parameters under CnB cKO conditions in comparison with the control.

(F) Axonal length, p = 0.0025.

(G) Axonal node, p = 0.0242.

(H) Dendritic length, p = 0.0101.

(I) Dendritic node, p = 0.0242.

(J–M) Morphometric analysis of VIP+ interneurons under control and CnB cKO conditions does not show any significant change in any parameter.

(J) Axonal length, p = 0.5317.

(K) Axonal node, p = 0.4127.

(L) Dendritic length, p = 0.4127.

(M) Dendritic node, p = 0.3333. Mean ± SEM, Mann-Whitney test. See also Figure S6.

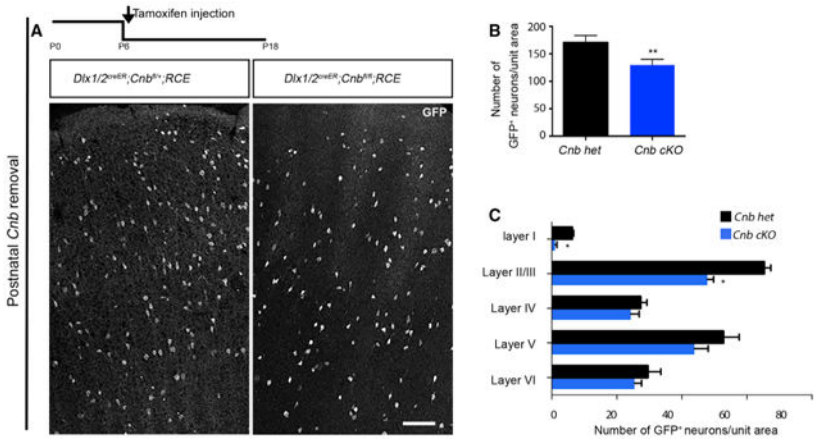

Figure 7. Timing of CaN Removal Is Critical in Regulating Cell Death

(A) Experimental design and representative image of coronal sections showing the distribution of GFP+ interneurons upon conditional removal of Cnb using an inducible driver line, Dlx1/2creER, reported by EGFP expression by using RCE::lox P. Tamoxifen was injected at P5, and the brains were analyzed at P18.

(B) Quantification of the number of EGFP+ interneurons shows a reduction in cell density upon conditional removal of Cnb. n = 4, p = 0.0050 (paired t test).

(C) Quantification of the layer distribution using the Dlx1/2creER driver line shows a decrease in the density in superficial layers. Scale bar, 100 μm. See also Figure S7.